

A Facile Synthesis of Fe-doped Zirconium Oxide Nanoparticles for Enhancement of Rhodamine B Dye Degradation

Yuanfeng Hui*, Shuyue Zhang

College of resources and environment engineering, Jilin Institute of Chemical Technology, Jilin 132022, China

*E-mail: huiyuranbaba@sina.com

Received: 5 March 2021 / Accepted: 13 April 2021 / Published: 30 April 2021

This work presents a synthesis of undoped and Fe-doped zirconium oxide nanoparticles (ZrO₂ NPs) as photocatalyst for degradation of Rhodamine B dye (RB). The undoped and doped ZrO₂ photocatalysts were successfully synthesized using co-precipitation process. Structural and morphological studies using XRD and FESEM showed that spherical shapes of undoped and Fe-doped ZrO₂ NPs prepared in high crystallinity and tetragonal phase. The optical characterization of photocatalysts using UV–Vis absorbance spectra revealed that the band gap was increased with increasing the dopant concentration. The band gap values of 4.98, 4.44, 4.29, 4.05 and 3.88 eV were obtained for undoped ZrO₂, 2wt%, 5wt%, 8wt% and 10wt% Fe-doped ZrO₂ NPs, respectively, which indicates narrowing of band gap with increasing the Fe concentration. The results of photodegradation studies showed that the complete removal of 100 mg/l RB was obtained after 55 minutes UV irradiation for the 8wt% Fe-doped ZrO₂. The maximum photodegradation efficiency on 8wt% Fe-doped ZrO₂ than undoped ZrO₂ can be associated with the presence of Fe³⁺ ions that can act as a sink and trap and transfer holes and electrons to minimize recombination of photoexcited electrons and holes. The stability response of 8wt% Fe-doped ZrO₂ photocatalyst to degradation of Rhodamine B under UV irradiation showed that the photocatalyst had great recycling stability.

Keywords: Fe-doped zirconium oxide Nanoparticles; Photocatalyst; Rhodamine B; Photodegradation; Cycle voltammetry

1. INTRODUCTION

Rhodamine B (RB, C₂₈H₃₁ClN₂O₃) is a chemical compound dye for fluorescence staining of bacteriological smears and histological tissue sections of human origin [1, 2]. The dyes consist of RB fluoresce, thus making the detection of the same becomes easy in fluorometers, flow cytometers and enzyme-linked immunosorbent assay [3]. Moreover, this dye is increasingly used for printing and dyeing purposes in textile, plastic, paper, paints and leathers industries, and pharmaceutical companies [4, 5]. However, side effects related to utilization of RB, owing to its carcinogenic properties, restrain

the growth of the market. This dye is injurious if swallowed and causes serious eye damage. Reports also show that it is harmful to aquatic life with long lasting effects [6, 7].

Therefore, researches were focused on removal of RB from industrial wastewater using various treatment strategies such as ozone-based advanced oxidation, electro-fenton, adsorption, sonication, peroxicoagulation, ion flotation, sonochemical degradation and photodegradation [8-10]. Recently, photodegradation, based on a combination of metallic particles and semiconductor photocatalysts such as TiO₂, ZnO, CdS, Fe₂O₃, GaP, ZnS and CuO have been studied as a new approach for promote of treatment by UV-visible light irradiation. The metallic dopants such as Au, Cu, Pt, Fe and Ag can greatly absorb visible through localized photocatalyst because metallic particles can act as electron traps and active sites [8, 11, 12].

The metallic dopants can act as collective oscillation of electrons at the photocatalysts matrix [13]. For example, Bi and Cao [8] showed that the Mn doping in TiO₂ photocatalyst not only led to decrease of recombination rate of photogenerated charges but also could narrow the band gap of doped photocatalysts which promotes photoactivity of TiO₂ in visible light range. Alshammari et al. [14] showed that supported Au nanoparticles on TiO₂ were improved the photodegradation of RB under UV light irradiation due to the strong reflection of UV irradiation by Au nanoparticles over TiO₂ support. Malika and Sonawane [15] also studied the ultrasonic photodegradation of RB dye using aqueous based Bi-metal doped TiO₂ and showed that the Bi-metal addition can improve the adsorption surface area and porosity of the photocatalyst.

Therefore, this study represented the effect of the Fe dopant on photodegradation properties of ZrO₂ nanoparticles for treatment of RB dye.

2. EXPERIMENT

All chemicals in high purity were purchased from Sigma-Aldrich. In order to synthesis of Fe-doped ZrO₂ nanoparticles photocatalysts, the ZrO₂ NPs were prepared in co-precipitation process which included to preparation the aquatic solution of 0.05 M ZrOCl₂.8H₂O as precursor and 1mM ammonia in equal volume ratio. Then, FeCl₃.6H₂O was added to the solution to obtain doping content of 2, 5, 8 and 10 wt%. For completing the process, the solution was heated for 60 minutes at 50°C in a water bath under continuous stirring at 600 rpm. After then, the resulting nanoparticles in solution were collected after being centrifuged at 2000 rpm, and followed by washing with deionized water and ethanol, respectively. The obtained Fe-doped ZrO₂ nanoparticles were dropped on Si substrates (for photodegradation studies) and glassy carbon electrodes (for electrochemical studies), and dried in oven at 80°C for 5 hours and calcined in a tube furnace at 450°C for 60 minutes.

The field emission scanning electron microscopy (FESEM, FEI-Nova 200 Nanolab, Hillsboro, OR, USA) was applied to study surface morphology of undoped and Fe-doped ZrO₂ photocatalysts. X-ray diffraction (XRD, Bruker diffractometer D8 Focus operated at 35kV and 0.025A with ($\lambda = 1.5406 \text{ \AA}$) Cu K α radiation was used to consider the crystal structure of prepared NPs. The optical absorption spectroscopy was recorded using a UV-visible spectrometer (Ocean Optics SD2000). Electrochemical study using the cycle voltammetry (CV) assessment were conducted on

AUTOLAB electrochemical workstation into conventional three-electrode electrochemical cell which included Ag/AgCl as reference, Pt as counter and the prepared Fe-doped ZrO₂ nanoparticles on glassy carbon electrode as working electrodes. CV measurements were done in 0.1 M phosphate buffer solutions (PBS) containing 5mM [Fe(CN)₆]^{3-/4-}. The 0.1M PBS prepared from 0.1M H₃PO₄ and 0.1 M NaH₂PO₄. 100 mg/l of RB solution was ultrasonically prepared. Before the measurement, the RB solution was kept for 40 minutes in darkness to achieve adsorption-desorption equilibrium. The photodegradation process was conducted under UV lamp mercury 300 W and 500 W Xe-lamp irradiations. The absorption spectra of the RB was recorded using a UV-Vis spectrometer. The RB concentration was determined by monitoring the changes in the absorbance peak at 550 nm.

3. RESULTS AND DISCUSSION

The XRD pattern of ZrO₂, 2wt%, 5wt%, 8wt% and 10wt% Fe-doped ZrO₂ are revealed in Figure 1. All XRD patterns shows strong peaks at $2\theta = 30.29^\circ, 35.18^\circ, 50.47^\circ, 60.28^\circ, 63.01^\circ$ and 74.55° which related to high crystallinity and formation of tetragonal zirconia phase with planes of (101), (110), (112), (211), (202) and (220), respectively according to JPCDS card No. 80-2155. There are not any peaks related to impurities from dopants in doped samples which indicated incorporation of dopant ions in ZrO₂ structure and stabilized the high-symmetry tetragonal phase of ZrO₂. Moreover, the ionic radius of Zr⁴⁺ ions (0.72 Å) is slightly larger than that of Fe³⁺ ions (0.63 Å) which implies an easy substitution of dopant in Zr⁴⁺ in the ZrO₂ lattice. The crystallite sizes of undoped and doped samples were calculated using Debye-Scherrer formula as following equation [16]:

$$D = \frac{0.9\lambda}{\beta \cos \theta} \quad (1)$$

Where D is the crystallite size, λ is the X-ray wavelength, θ is the Bragg angle (radians), and β is the line broadening at half the maximum intensity (radians). The calculation for the (101) plane illustrates that the crystallite sizes of 16.51, 17.08, 18.78, 21.49 and 23.98 nm are obtained for undoped ZrO₂, 2wt%, 5wt%, 8wt% and 10wt% Fe-doped ZrO₂ NPs, respectively. As observed, the crystallite size is improved with increasing the doping concentration. The particle size plays an important role in photon absorption on photocatalyst [17]. Smaller particle sizes on photocatalyst shows the shorter diffusion length for photogenerated charge carriers to reach the surface before reaching surface reaction sites and recombination [18-20].

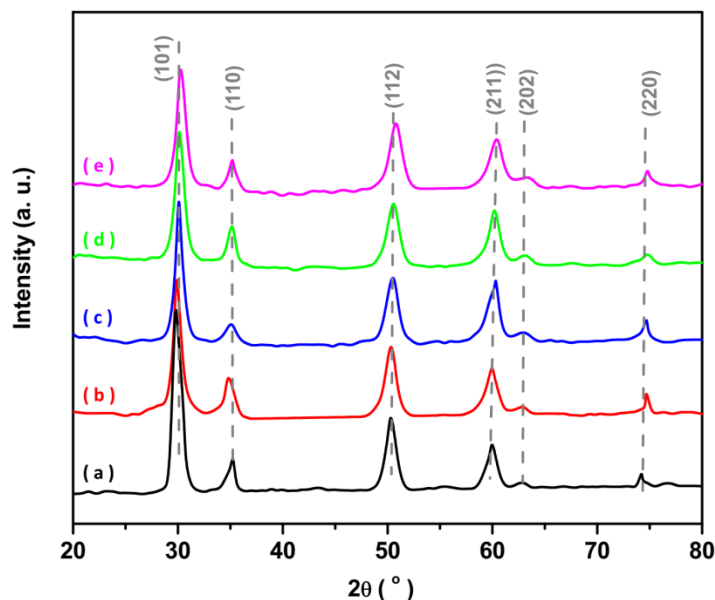


Figure 1. The XRD patterns of (a) undoped ZrO_2 , (b) 2wt%, (c) 5wt%, (d) 8wt% and (e) 10wt% Fe-doped ZrO_2 .

The FESEM images of undoped and Fe-doped ZrO_2 nanoparticles shown in Figure 2. As observed, the fine grains of undoped and doped ZrO_2 nanoparticles are synthesized in uniform size. As seen, spherical ZrO_2 nanoparticles homogeneously distributed on photocatalysts surface. The average particle sizes of 55 and 80 nm are obtained for undoped ZrO_2 and Fe-doped ZrO_2 samples, respectively.

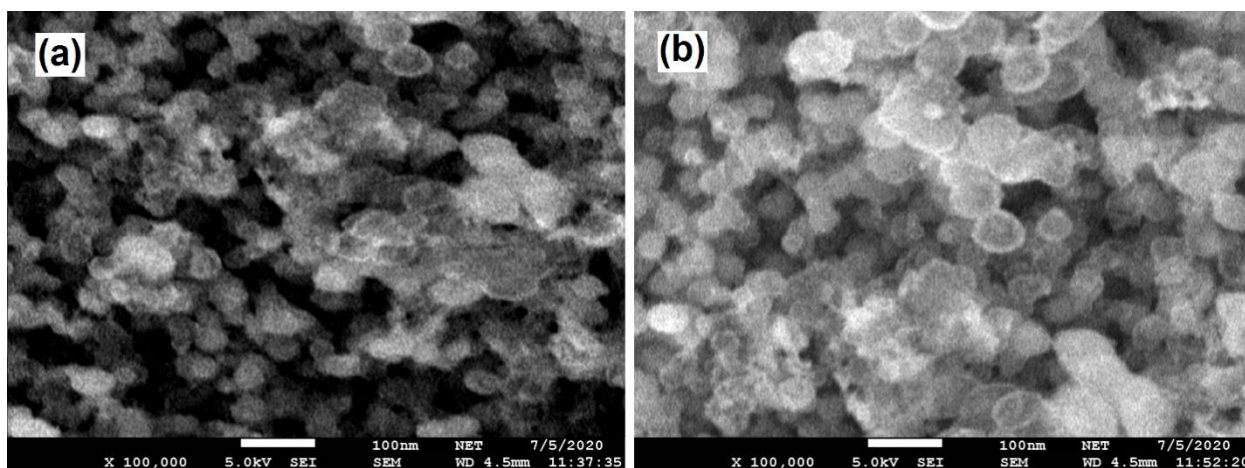


Figure 2. The FESEM images of (a) undoped ZrO_2 nanoparticles and (b) Fe-doped ZrO_2 nanoparticles.

Optical properties of prepared photocatalyst were studied using UV–Vis absorbance spectra. As observed from Figure 3a, the spectra displays sharp and noticeable absorption peak at 217 nm which is attributed to interband transitions that it indicated to band-to-band electron transitions from the valence to the conduction band. The strong and absorption bands are observed for undoped and doped ZrO_2 which implies to nano-scale of particles that it provides a high surface to volume ratio and enhances defects distribution on photocatalyst surfaces [21, 22]. The absorption intensity is increased

with increasing the dopant concentration. Moreover, the absorption tail is shifted toward a lower photon energy with increasing the doping concentration due to increasing the contribution of the metallic absorption site in ZrO₂ lattice [23, 24]. Figure 3b shows the results of band gap (E_g) calculation of samples using Tauc's method according the following equation:

$$(\alpha h\nu)^2 = A(h\nu - E_g) \quad (2)$$

Where α is absorption coefficient, $h\nu$ is photon energy, A is constant. Band gap values are determined from the extrapolation of the linear fit for the Tauc plot onto the energy axis. Result shows that the band gap values of 4.98, 4.44, 4.29, 4.05 and 3.88 eV are obtained for undoped ZrO₂, 2%, 5%, 8% and 10% Fe-doped ZrO₂ NPs, respectively, which demonstrated to narrowing of band gap value with increasing the Fe concentration. The substitution of Fe ions replaced by Zr⁴⁺ ions into the host lattice creates some new electronic states into the ZrO₂ band gap. These new states exist near the lower edge of the conduction band forming a new lowest unoccupied molecular orbital [25]. Studies showed that the band gap and the valence band edge of the undoped ZrO₂ NPs are at ≈ 5.0 eV and 3.28 eV, respectively, which caused to the conduction band minimum and conduction band minimum would be located at ≈ -1.72 eV [26]. For Fe doped ZrO₂, the valence band maximum and conduction band minimum are located at ≈ 1.21 eV and -1.35 eV, respectively, this difference leads to the narrowing of the band gap [26].

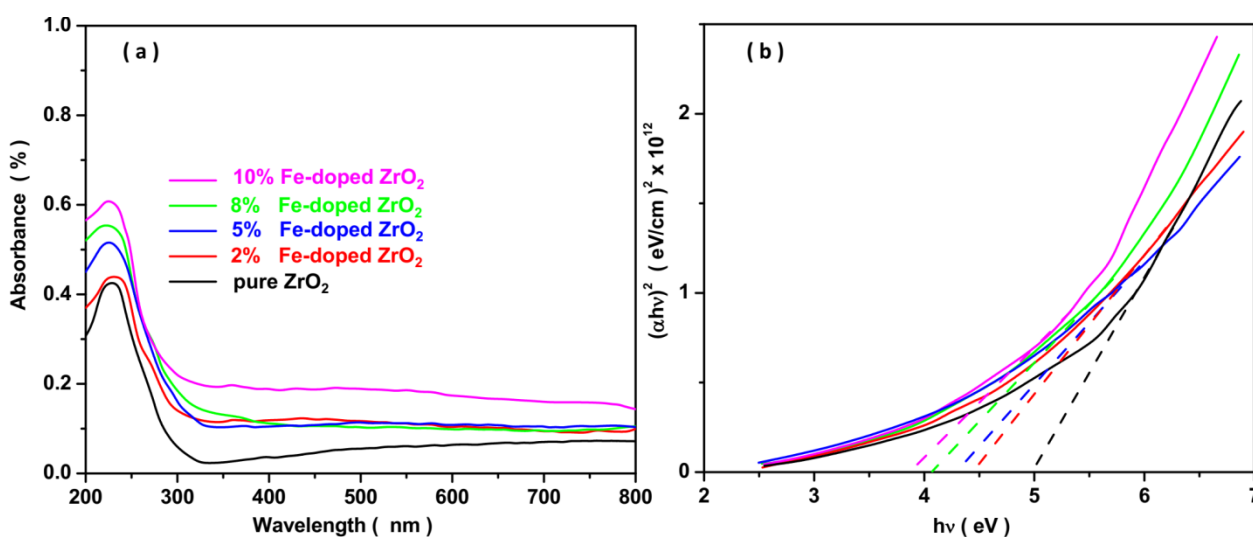


Figure 3. (a) UV-Visible absorption spectrum and (b) Taucs plot of undoped ZrO₂, 2%, 5%, 8% and 10% Fe-doped ZrO₂ NPs.

Figure 4 shows the recorded CVs of undoped and Fe-doped ZrO₂ nanoparticles 0.1 M PBS pH 7 containing 5 mM [Fe(CN)₆]^{3-/4-} as redox active material at scan rate of 20 mV/s. As observed, the anodic and cathodic peak currents are 0.37 and 0.03 V for pure and doped ZrO₂ nanoparticles, respectively. The currents of redox peaks are increased with increasing the dopant concentration in ZrO₂ nanoparticles due to enhancement of conductivity which results in better electron transfer and charge separation [27, 28]. The lower charge transfer resistance can accelerate the interfacial charge-

transfer process and provides more contribution to the enhanced photocatalytic activity via the easy transfer of charge. Therefore, the doped ZrO₂ nanoparticles can possess an enhanced photocatalytic activity as compared to the pure ZrO₂ [29-31].

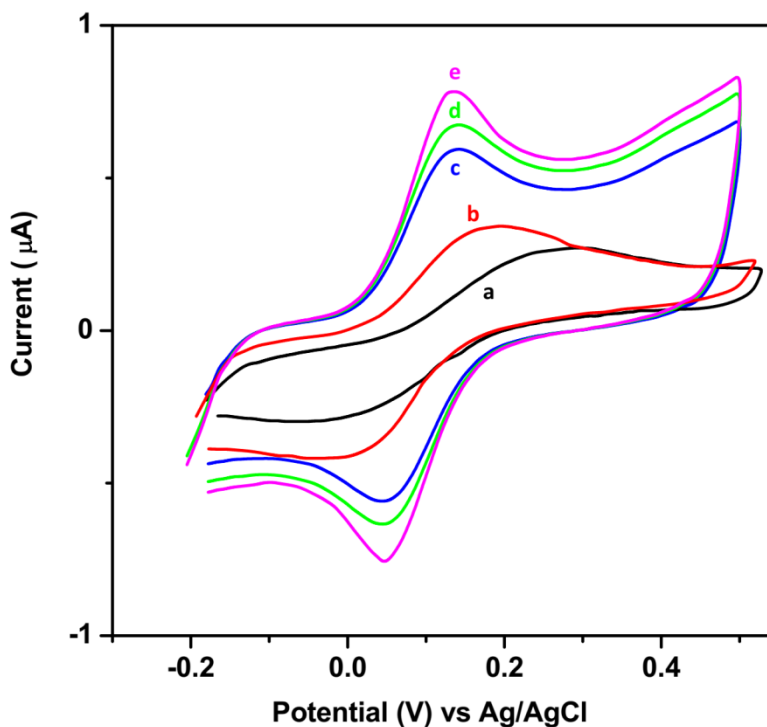


Figure 4. The recorded CVs of (a) undoped ZrO₂, (b) 2wt%, (c) 5wt%, (d) 8wt% and (e) 10wt% Fe-doped ZrO₂ in 0.1 M PBS pH 7 containing 5 mM [Fe(CN)₆]^{3-/4-} as redox active material at scan rate of 20 mV/s.

In order to investigation of dopant concentration on the degradation of 100 mg/l RB, the degradation efficiencies of RB on undoped ZrO₂, 2%, 5%, 8% and 10% Fe-doped ZrO₂ photocatalysts and without photocatalyst (blank) under UV and visible lights illuminations are shown in Figure 5a and 5b, respectively. The first 40 minutes, all samples were examined at dark conditions to study the degradation rate in darkness. It demonstrated that the degradation less than 0.8% occurred in the first 40 minutes. Thus, the RB solutions were kept in dark for 40 minutes to dark to reach the balance of adsorption-desorption. Moreover, it is observed from Figure 5a, the complete removal of RB is obtained at 55 and 70 minutes UV irradiation for the 8% and 10% Fe-doped ZrO₂. It is suggested that the smallest particles size in undoped and Fe-doped ZrO₂ shows the prominent effects to photodegradation under UV because of supporting the shortest diffusion length of photogenerated charge carriers and decrease the recombination rate [32], which in agreement to results of XRD and FESEM characterizations. The maximum photodegradation efficiency on 8% Fe-doped ZrO₂ than undoped ZrO₂ can be attributed to the Fe³⁺ ions that they act as a sink and trap and transfer holes and electrons to minimize recombination of photoexcited electrons and holes [33]. The results photodegradation measurements under visible lights illumination in Figure 5b reveal that the 8% and 10% Fe-doped ZrO₂ have the maximum rate of RB degradation and 100% degradation efficiencies are

obtained after 150 minutes visible lights illumination that these rates showed the removal rate is decreased toward that under UV illumination.

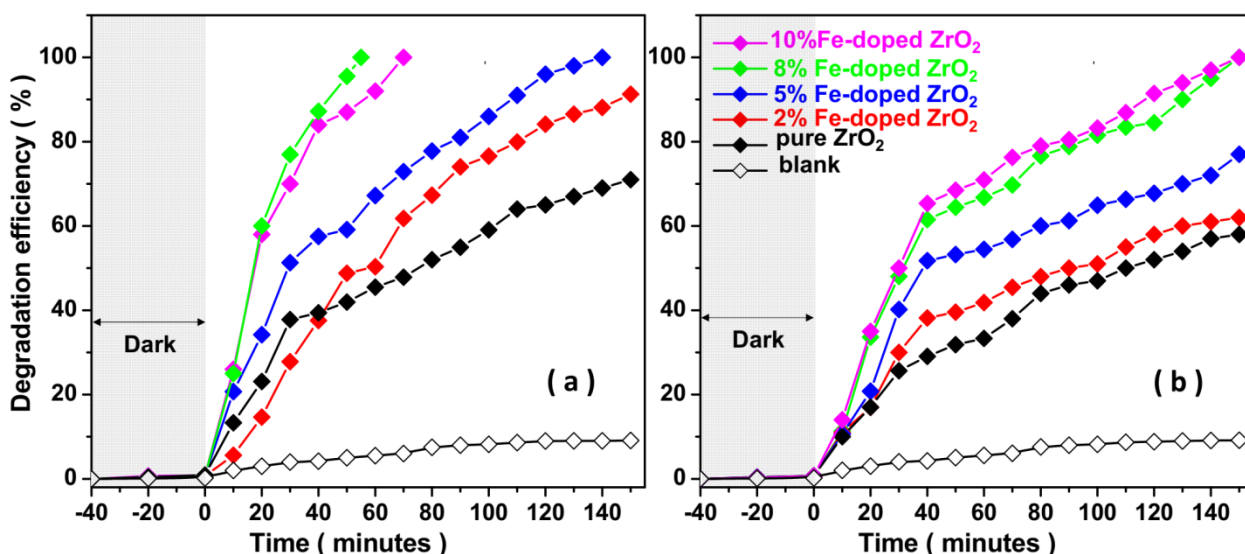


Figure 5. Photodegradation efficiency of 100 mg/l RB on undoped ZrO₂, 2%, 5%, 8% and 10% Fe-doped ZrO₂ photocatalysts and without photocatalyst (blank) under (a) UV and (b) visible lights illuminations.

Table 1. Comparison the results of photodegradation of this study with other reported photocatalyst for degradation of RB.

Photocatalyst	RB content (mg/l)	Light source	Degradation time (minute)	Degradation efficiency (%)	Ref.
8% Fe-doped ZrO ₂	100	UV visible	55 70	100 100	This work
Calcined TiO ₂ nanoparticles	10	UV	270	100	[35]
Cerium doped TiO ₂	0.5	UV	120	98	[36]
TiO ₂ @rGO,	30	UV	60	97	[37]
P doped TiO ₂	12	Solar light	30	95	[38]
Fe doped TiO ₂ /rGO	20	visible	120	91	[39]
Zirconium Phosphate/Silver Bromide	0.73	UV-visible	12	100	[40]
Rh doped TiO ₂	10	visible	180	95	[41]
Cobalt doped hydroxyapatite	40	UV-visible	12	93.3	[42]
TiO ₂ /nitrogen doped graphene quantum dots	10	visible	180	95	[43]

The degradation rates under visible are significantly decreased on all prepared photocatalysts toward that under UV illumination. Very poor degradation are observed on the undoped ZrO₂ under visible irradiation (degradation efficiency of 58% after 150 minutes) due its wide band gap that it limits its photoactivity to the UV irradiation range wavelength where the electron can absorb adequate energy to transition from the valence band to the conduction band [34]. These results demonstrate the narrowing band gap and creation of a new energy level above the original valence band of ZrO₂ under

doping process lead to 8% and 10% Fe-doped ZrO_2 show the great the photo-absorption, separation, transfer of photo-induced carriers under UV and visible light irradiation, which in agreement to results of optical studies.

The results of the photodegradation study are compared with other reported photocatalyst for degradation of RB in Table 1. As observed that the significant photodegradation rate of 100 mg/l RB on 8wt% Fe-doped ZrO_2 photocatalyst which is attributed to nano-scale of particles that it provides the high surface area-to-volume ratio and enhances defects distribution on the photocatalyst surface. Moreover, the doping process can create new energy levels above the original valence band of ZrO_2 which act as a sink and trap and transfer holes and electrons to minimize recombination of photoexcited electrons and holes.

Figure 6a shows the UV-vis absorption spectra of 100 mg/l RB on 8% Fe-doped ZrO_2 photocatalyst. It can be observed that the intensity of the absorption peaks at 550 nm continuously decreases during the photodegradation reactions which similar to reported results of RB degradation over zirconia incorporated titania nanoparticles [44]. The peak position is not changed and the peak disappears after 55 minutes degradation. Figure 6b shows the stability response of 8wt% Fe-doped ZrO_2 photocatalyst to degradation of Rhodamine B under UV irradiation. It can be observed that the photocatalytic activity does not change after 4 cycles that it demonstrates the photocatalyst excellent recycling and structural stability.

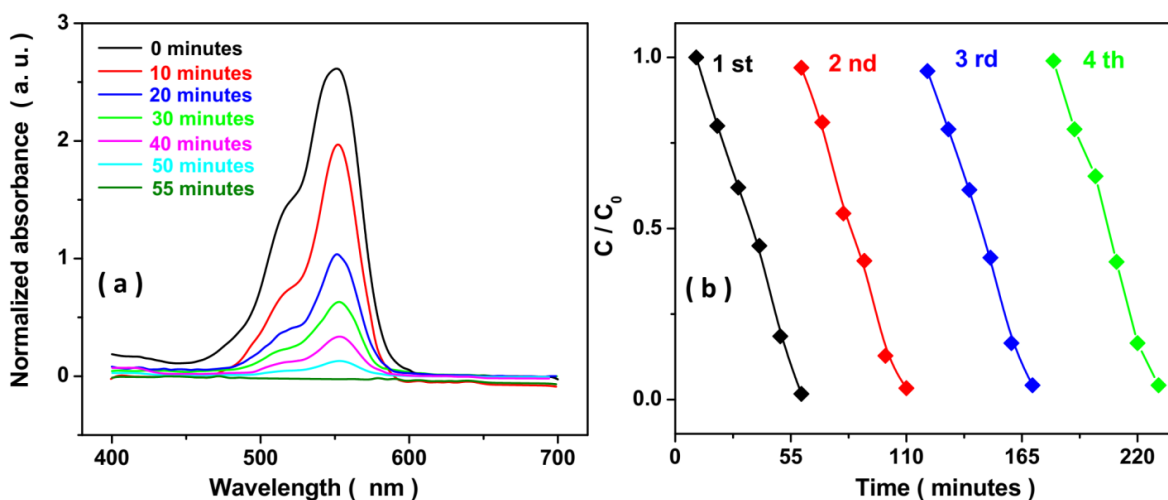


Figure 6. (a) UV–Vis spectra of photocatalytic degradation reaction of 100 mg/l RB with respect to different irradiation times by 8% Fe-doped ZrO_2 photocatalyst. (b) Stability response of 8wt% Fe-doped ZrO_2 photocatalyst to degradation of Rhodamine B under UV irradiation.

4. CONCOUSION

This study conducted on the synthesis of Fe-doped ZrO_2 NPs as photocatalyst for degradation of RB dye. The undoped and doped ZrO_2 photocatalysts were prepared by co-precipitation process. The structural and morphological studies showed that spherical shaped nanoparticles synthesized in high crystallinity and tetragonal phase. The UV–Vis absorbance spectra showed that the band gap was

increased with increasing the dopant concentration and the band gap values of 4.98, 4.44, 4.29, 4.05 and 3.88 eV were obtained for undoped ZrO₂, 2%, 5%, 8% and 10% Fe-doped ZrO₂ NPs, respectively, which demonstrated narrowing of band gap with increasing the Fe concentration. The results of photodegradation showed that the complete removal of 100 mg/l RB was obtained after 55 minutes UV irradiation for the 8% Fe-doped ZrO₂. The maximum photodegradation efficiency on 8wt% Fe-doped ZrO₂ than undoped ZrO₂ can be related to the Fe³⁺ ions that act as a sink and trap and transfer holes and electrons to reduce recombination of photoexcited electrons and holes. The stability response of 8wt% Fe-doped ZrO₂ photocatalyst to degradation of Rhodamine B under UV irradiation showed that the photocatalyst had an excellent recycling and structural stability.

References

1. N. Tara, S.I. Siddiqui, G. Rathi, S.A. Chaudhry and A.M. Asiri, *Current Analytical Chemistry*, 16 (2020) 14.
2. H. Karimi-Maleh, Y. Orooji, A. Ayati, S. Qanbari, B. Tanhaei, F. Karimi, M. Alizadeh, J. Rouhi, L. Fu and M. Sillanpää, *Journal of Molecular Liquids*, 329 (2021) 115062.
3. A. Petropoulou, S. Kralj, X. Karagiorgis, I. Savva, E. Loizides, M. Panagi, T. Krasia-Christoforou and C. Riziotis, *Scientific reports*, 10 (2020) 1.
4. B. Campanella, J. Botti, T. Cavaleri, F. Cicogna, S. Legnaioli, S. Pagnotta, F. Poggialini, T. Poli, D. Scalarone and V. Palleschi, *Microchemical Journal*, 152 (2020) 104292.
5. J. Rouhi, S. Kakooei, M.C. Ismail, R. Karimzadeh and M.R. Mahmood, *International Journal of Electrochemical Science*, 12 (2017) 9933.
6. W. Wang, Y. Du, Z. Xiao, Y. Li, B. Li and G. Yang, *Analytical Sciences*, 33 (2017) 715.
7. C. Liu and J. Rouhi, *RSC Advances*, 11 (2021) 9933.
8. J. Bi and X. Cao, *International Journal of Electrochemical Science*, 16 (2021) 210340.
9. C. Yang, H. Xie, Z. Wang, Y. Tan and N. Wang, *International Journal of Electrochemical Science*, 16 (2021) 151058.
10. H. Karimi-Maleh, M. Alizadeh, Y. Orooji, F. Karimi, M. Baghayeri, J. Rouhi, S. Tajik, H. Beitollahi, S. Agarwal and V.K. Gupta, *Industrial & Engineering Chemistry Research*, 60 (2021) 816.
11. G.-Y. Yao, Q.-L. Liu and Z.-Y. Zhao, *Catalysts*, 8 (2018) 236.
12. H. Karimi-Maleh, M.L. Yola, N. Atar, Y. Orooji, F. Karimi, P.S. Kumar, J. Rouhi and M. Baghayeri, *Journal of colloid and interface science*, 592 (2021) 174.
13. H. Karimi-Maleh, S. Ranjbari, B. Tanhaei, A. Ayati, Y. Orooji, M. Alizadeh, F. Karimi, S. Salmanpour, J. Rouhi and M. Sillanpää, *Environmental Research*, 195 (2021) 110809.
14. A. Alshammari, A. Bagabas and M. Assulami, *Arabian Journal of Chemistry*, 12 (2019) 1406.
15. M. Malika and S.S. Sonawane, *Sustainable Energy Technologies and Assessments*, 44 (2021) 100980.
16. H. Savaloni and R. Savari, *Materials Chemistry and Physics*, 214 (2018) 402.
17. T. Hisatomi, K. Takanabe and K. Domen, *Catalysis Letters*, 145 (2015) 95.
18. L. Li, P.A. Salvador and G.S. Rohrer, *Nanoscale*, 6 (2014) 24.
19. R. Savari, H. Savaloni, S. Abbasi and F. Placido, *Sensors and Actuators B: Chemical*, 266 (2018) 121447.
20. K. Maeda, *Journal of Photochemistry and Photobiology C: Photochemistry Reviews*, 12 (2011) 237.

21. D. Li, H. Song, X. Meng, T. Shen, J. Sun, W. Han and X. Wang, *Nanomaterials*, 10 (2020) 546.
22. F. Chahshouri, H. Savaloni, E. Khani and R. Savari, *Journal of Micromechanics and Microengineering*, 30 (2020) 075001.
23. F. Huang, A. Yan and H. Zhao, *Semiconductor photocatalysis-materials, mechanisms and applications*, (2016) 31.
24. R. Hassanzadeh, A. Siabi-Garjan, H. Savaloni and R. Savari, *Materials Research Express*, 6 (2019) 106429.
25. S. Bingham and W.A. Daoud, *Journal of Materials Chemistry*, 21 (2011) 2041.
26. M. Xiao, Y. Li, Y. Lu and Z. Ye, *Journal of Materials Chemistry A*, 3 (2015) 2701.
27. R. Savari, S. Soltanian, A. Noorbakhsh, A. Salimi, M. Najafi and P. Servati, *Sensors and Actuators B: Chemical*, 176 (2013) 335.
28. B. Pant, G.P. Ojha, Y.-S. Kuk, O.H. Kwon, Y.W. Park and M. Park, *Nanomaterials*, 10 (2020) 1960.
29. B. Surendra, *Journal of Science: Advanced Materials and Devices*, 3 (2018) 44.
30. Z. Savari, S. Soltanian, A. Noorbakhsh and A. Salimi, *Electrochemical Society Iran*, 9 (2013) 1.
31. J. Rouhi, S. Kakooei, S.M. Sadeghzadeh, O. Rouhi and R. Karimzadeh, *Journal of Solid State Electrochemistry*, 24 (2020) 1599.
32. K. Maeda, H. Terashima, K. Kase and K. Domen, *Applied Catalysis A: General*, 357 (2009) 206.
33. H. Song, Y. Li, Z. Lou, M. Xiao, L. Hu, Z. Ye and L. Zhu, *Applied Catalysis B: Environmental*, 166 (2015) 112.
34. M.A. Wahba and S.M. Yakout, *Journal of Sol-Gel Science and Technology*, 92 (2019) 628.
35. M.M. Mahlambi, A.K. Mishra, S.B. Mishra, R.W. Krause, B.B. Mamba and A.M. Raichur, *Journal of thermal analysis and calorimetry*, 110 (2012) 847.
36. J. Xiao, T. Peng, R. Li, Z. Peng and C. Yan, *Journal of Solid State Chemistry*, 179 (2006) 1161.
37. M.H.H. Ali, A.D. Al-Afify and M.E. Goher, *The Egyptian Journal of Aquatic Research*, 44 (2018) 263.
38. Y. Lv, L. Yu, H. Huang, H. Liu and Y. Feng, *Journal of Alloys and Compounds*, 488 (2009) 314.
39. A.A. Isari, A. Payan, M. Fattahi, S. Jorfi and B. Kakavandi, *Applied Surface Science*, 462 (2018) 549.
40. M. Pica, S. Calzuola, A. Donnadio, P.L. Gentili, M. Nocchetti and M. Casciola, *Catalysts*, 9 (2019) 1.
41. E.A. Obuya, W. Harrigan, T. O'Brien, D. Andala, E. Mushibe and W.E. Jones, *MRS Online Proceedings Library Archive*, 1352 (2011) 113.
42. Y. Pang, L. Kong, D. Chen, G. Yuvaraja and S. Mehmood, *Journal of hazardous materials*, 384 (2020) 121447.
43. N.-Q. Ou, H.-J. Li, B.-W. Lyu, B.-J. Gui, X. Sun, D.-J. Qian, Y. Jia, X. Wang and J. Yang, *Catalysts*, 9 (2019) 345.
44. C.-C. Ou, C.-S. Yang and S.-H. Lin, *Catalysis Science & Technology*, 1 (2011) 295.